

A Hybrid Bondline Concept for Bonded Composite Joints

T. Löbel^{1*}, D. Holzhüter¹, M. Sinapius^{2,1}, C. Hühne^{1,2}

¹ DLR, German Aerospace Center Lilienthalplatz 7, 38108 Braunschweig, Germany

² Technische Universität Braunschweig, Institute of Adaptronics and Function Integration, 38106 Braunschweig, Germany

Abstract

Based on the experience in the past and the occurrence of in-service damages, the authorities restrict today the application of adhesive bonding of composite structures for aircraft applications. However, certification limitations can be overcome if occurring disbonds within a bond are stopped by implemented design features, so called disbond stopping features. Consequently, a novel bondline architecture for bonded composite joints is proposed. By implementing a distinct rather ductile thermoplastic phase, a physical barrier for growing disbonds is obtained and thus a fail-safe design, respectively. Moreover, the joint is established by using two different joining technologies, namely adhesive bonding and thermoset composite welding. A sophisticated manufacturing technique is developed for the hybrid bondline concept to achieve a high strength joint. The joint's quality is examined by means of several analytical methods like microsections, scanning electron microscopy (SEM), and energy-dispersive X-Ray (EDX) analysis. Additionally, the mechanical performance is evaluated by static Double Cantilever Beam (DCB) and Single Lap Shear (SLS) tests.

Keywords: Adhesive bonding, Disbond stopping, Double cantilever beam test, Single lap shear test, CFRP joints

1. Introduction

1.1. Today's Usage and Limitations of Bonded Composite Joints

Due to their superior weight to strength ratio, composite materials are increasingly used in aircraft primary structures. This tendency becomes evident with the composite usage for Boeings 787 and Airbus A350XWB exceeding 50%. The implementation of more CFRP load-bearing parts demands efficient solutions in terms of joining technology.

With bolting on the one hand and adhesive bonding on the other, there are two joining techniques available for thermoset composites which are the majority of composites used for aeronautical applications. From a mechanical perspective, adhesive bonding is the favorable joining technique for several reasons. Adhesive bonds lead to weight reduction, offer a more

uniform load distribution, are capable of joining thin-walled parts and minimize material weakening. The presence of fasteners has a noticeable impact on the part design and could even be a key dimensioning factor. Thus, fasteners hamper the full lightweight potentials of composites [1]. Therefore, the development of adhesive bonds being capable for certification is of high interest.

For civil aircraft, bonding of composites is well-established for various secondary joints. Airbus' A380 features bonded joints for instance in the rear pressure bulkhead, the ailerons, the vertical tail plane and the radome as illustrated in Figure 1 [2]. For the latest aircraft of the Airbus family (Airbus A350XWB), a large share of stiffeners are (composite to composite) bonded joints leading to an overall bondline length of about 5 km per aircraft [3].

However, due to certification requirements (see Section 1.3) the implementation of bonded joints in aircraft composite structures is still limited to secondary joints or combined with so called "chicken rivets" if

*Corresponding author. fax: +49 531 295 3035.

Email address: thomas.loebel@dlr.de (T. Löbel¹)

used for primary joints. Those additional fasteners have to be capable to carry limit load in case of a global failure of the bondline [3]. Design benefits that come along with adhesive bonding do not come into effect, since fastening elements must be taken into account for part design. Thus, up to now the potential of adhesive bonding is not used to its full extent. The main reasons for this limitation are briefly discussed below.

1.2. Reasons for Certification Limitations

The manufacturing process of structural bonded joints is influenced by many factors, e.g. surface treatment, adhesive curing cycle, curing conditions (e.g. pressure and temperature distribution), entrapped adherend's humidity, and many more. Those factors may affect the long-term durability of the joint [4]. Judging their impact on the joint's performance is complex and still subject of current research and scientific discussions. Due to the absence of technologies for testing the quality of a bonded joint to full extent, a rigorous quality management system is required.

In addition to manufacturing uncertainties, aging and fatigue life of bonded composite joints is still challenging to predict and also influenced by many factors (e.g. load level, strain rate and environmental conditions) [5–7]. Thorough investigations of the interaction between those factors and their impact on the joint's long-term durability are hampered by the necessity of cost-consuming and time-consuming experimental fatigue studies. Furthermore, in-service damages (e.g. impact events) could hardly be avoided and may lead to a noticeable decrease of the joint's strength [5; 8].

Eventually, all those factors led to a significant scatter in the performance of bonded composite joints in the past with some working well and some failing after short time in service [9]. Those experiences have caused a distrust towards adhesive bonding as joining technology.

1.3. Certification Requirements of Bonded Composite Joints

Based on experience in the past and the uncertainties mentioned above, the authorities, namely the Federal

Aviation Administration (FAA, USA) and the European Aviation Safety Agency (EASA, Europe), specify two major prerequisites that have to be met to achieve certification of bonded composite joints for primary structures [4; 10].

The manufacturing process must be specified, controlled and monitored and has to be carried out in a pre-defined manufacturing process window regarding influencing parameters. Consequently, influencing parameters and their tolerable deviations have to be determined. Despite a rigorous manufacturing quality management, one of the following methods has to be established to attain certification [4; 10]:

1. Disbonds greater than a pre-defined maximum must be prevented by design features. The allowed disbond maximum must be determined by analysis, test, or both.
2. Proof testing has to be executed for every production article to ensure that the joint can withstand the desired design loads.
3. The load-bearing capability of each joint must be determined by repeatable and reliable non-destructive inspection (NDI) methods.

Proof testing of each production specimen is not desirable in serial production of large composite structures since testing is very cost-intensive. An NDI method that sheds light on the strength of adhesive bonds is currently not available. Porosities or voids may be detected by established methods like ultrasonic scanning or thermography. However, giving evidence that proper adhesion is achieved is not possible today [11].

In the end, a promising approach is to establish disbond stopping design features. Those must be developed and incorporated in each bond to prevent a possible disbond reaching a critical extent. This initial situation is the major motivation for the developments that are made in the European project BOPACS of the Seventh Framework Program (FP7).

Several crack stopping approaches are under investigation within the project like the so called rivetless nut plates [12], small diameter pins [13] or surface modifications [14]. Another promising approach is the hybrid bondline concept which is introduced here.

The denotation *disbond* and *crack* are used synonymously in this work to describe the joint's (local) sep-

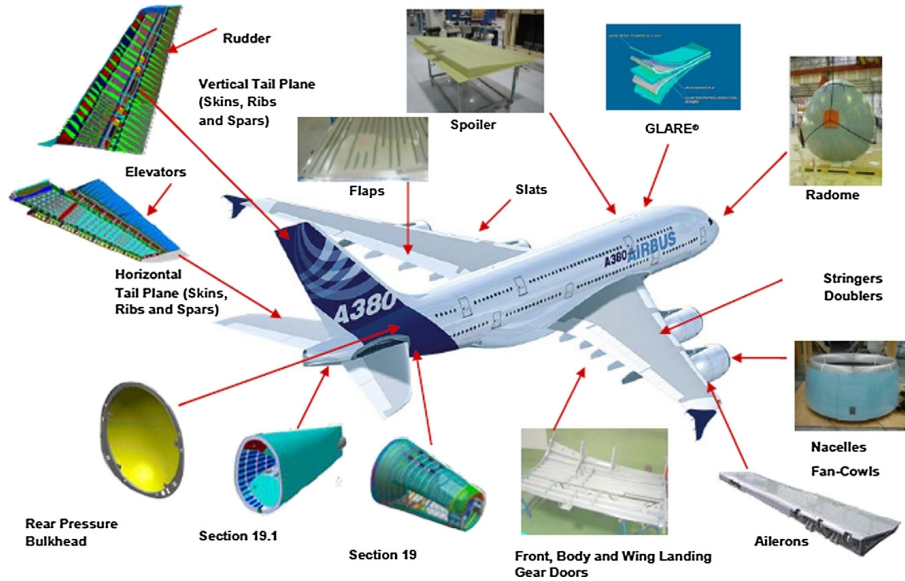


Figure 1: Usage of adhesive bonding in the Airbus A380 [2]

aration within the bondline.

2. The Hybrid Bondline Approach

2.1. Working Principle

Many conventional epoxy adhesives for aeronautical applications are toughness-modified in order to reduce undesired brittle behavior that inherently applies for pure epoxy systems. For instance, rubber particles could be used as toughening material as proposed by Ranta et al. and Kinloch et al. [15; 16]. However, adhesive toughening by incorporation of rubber or thermoplastic particles may lead to a degradation of stiffness and strength. Therefore, toughening may be seen as a compromise between ductile behavior of good nature and stiffness or strength, respectively. The concept that is introduced here avoids the unfavorable trade-off by a strict separation of both functions (toughness, and shear strength and stiffness for load transfer). This separation is achieved by dividing the bondline into several areas as shown in Figure 2. In contrast to toughening modifications, this concept is not an adhesive development as the epoxy adhesive remains unmodified.

On the one hand, a conventional high strength structural adhesive is used in phase I (Figure 2). Due to its high stiffness compared to phase II, major loads are carried by phase I. On the other hand, phase II

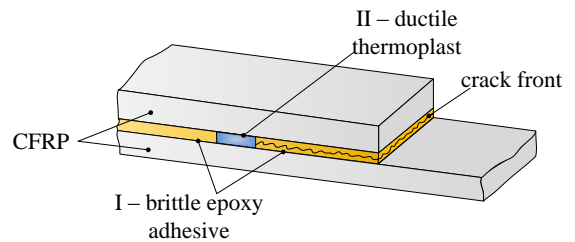


Figure 2: Concept introduction: principle alignment of both adhesives within the bondline for a doubler configuration (e.g. a stringer to skin joint)

shall be realized by implementation of a pure thermoplastic material showing superior ductility by nature. Accordingly, this physical barrier acts as disbond stopping feature within the bondline through a sharp change of materials. A new crack initiation would be needed for further crack growth which is unlikely due to the better fracture mechanical properties of the thermoplastic material.

Growing cracks are not just slowed down. Growing cracks shall be fully stopped.

Malkin et al. [17] introduced an analog selective toughening approach for the sake of damage tolerance by local incorporation of rubber particles. Growing cracks were sufficiently arrested after reaching the toughened area. However, in contrast to the ap-

proach here, toughening was applied between two laminate plies and not as damage tolerance design feature within an adhesive bond.

As shown in Figure 3 the disbond stopping feature (DSF) could be integrated multiple times strip-wise perpendicular to the major load direction and crack path, respectively. However, for the sake of simplicity, the investigations here focus on the implementation of just one crack stopping element as depicted in Figure 2.

Due to the thermoplast position in areas of low stresses for the doubler scenario, only minor stress concentrations are expected at the transition of both materials (see Section 4.4). Hence, the impact on the overall bond strength for an intact joint is expected to be small and tolerable. Furthermore, an enhanced load distribution is expected if a propagating crack reaches the area of the more ductile thermoplast. The position of the ductile material at the (new) overlap edge correlates to an often proposed design principle called *functionally graded bondline* [18] which is also known as *mixed-adhesive joint* [19]. Thereby, occurring stress peaks at the overlap edge are reduced as a result of the presence of material with lower stiffness at the edge and stiffer epoxy adhesive in the center as depicted in Figure 4. Consequently, the bond strength is increased and a new crack initiation is less likely.

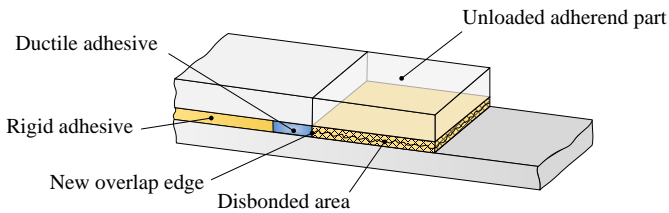


Figure 4: Mixed-adhesive configuration in case a crack reaches the disbond stopping area

The implementation of thermoplast material to get a functionally graded bondline could be used right from the beginning for doubler configurations by placing the tougher material at the overlap edges. However, this design optimization shall not be the focus of the work presented here. The main purpose of the tough thermoplast is to act as distinct crack stopper within the bondline.

Furthermore, innovation is achieved since the thermoplastic area shall be joint by thermoplastic welding. As the thermoplast is welded within the bondline, not only a combination of material properties is established, but a combination of two different joining techniques: adhesive bonding and thermoplast welding. For the weld the so called *thermoset composite welding* (TCW) [20] shall be used which is described in more detail in Section 2.2. Thus, the joint does not solely rely on adhesive bonding which is accompanied with manufacturing uncertainties as discussed in Section 1.2.

2.2. Manufacturing Concept

The joint manufacturing can be divided into four steps as shown in Figure 5. First, the thermoplast strips are put in place before curing of the adherend parts (Step I). The prepreg curing cycle is conducted as specified by the material data sheet [21]. A polytetrafluoroethylene (PTFE) release film between the plates surface and the steel tooling ensures a constant overall surface finish. As a strip of thermoplast is applied to an uncured prepreg surface and processed in a prepreg curing cycle, it is incorporated into the material during autoclaving. Hence, a plane surface is created due to the applied pressure (Step II).

Since the thermoplast's melting point matches the curing temperature of the CFRP, a strong bond is realized between the thermoplast and the composite's matrix system. For a similar approach it is assumed by Paton et al. [20] that a semi-interpenetrating polymer network is established between both materials, providing a molecular interlocking. Thereby, long thermoplastic molecules are entangled with cross-linked thermoset molecule chains as described by Deng et al. [22]. A similar approach is described in Hou's work [23] where an amorphous thermoplastic film as outermost layer of a thermoset composite is used to obtain a fusion bonded joint.

The thermoplastic strips are placed on both adherend surfaces. Thus, the strips face each other when both parts are joined. For all test specimens (see Section 4) strips of 10 mm in width are used for this process step.

In a third step (Figure 5), the actual bonding is conducted by placing the epoxy film adhesive on one adherend with the area of thermoplastic strips left

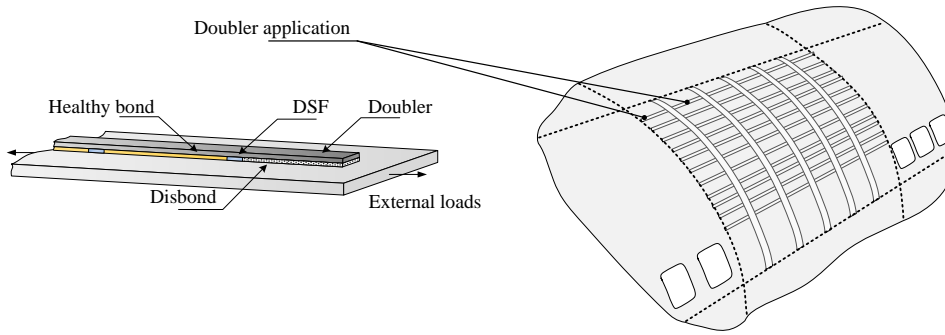


Figure 3: Principle alignment of the disbond stopping feature for a doubler configuration (e.g. stringer to skin)

open. Two additional strips of thermoplast with an overall thickness of 0.25 mm and 7 mm width are put in the area left open. Small adjustment errors of the strips are acceptable since the strips that are already placed within the prepreg have a slightly larger width of 10 mm (Figure 5). Therefore, a proper welding of the inserted strip shall be ensured.

In the final step IV, the adhesive is cured and the bond is thus established. Both, adhesive curing and thermoplastic welding are performed simultaneously. In doing so, all 4 thermoplastic strips are welded through coalescence of the material. The applied curing temperature of 180° C and pressure of 3.5 bar ensures proper welding at the interface of the thermoplastic layers. Pressure and temperature are maintained for 2 hours to allow complete polymerization of the epoxy adhesive.

In contrast to adhesive bonding, welding does not need surface pretreatment of the adherends. Applied heat causes the thermoplast to soften, while applied pressure causes the softened asperities to spread, resulting in a contact area development. The high temperatures at the interphase lead to interdiffusion of polymer chains, a process referred as *healing* [24]. Due to the homogenous polymer network, welded joints do not rely on adhesion at the material interphase.

2.3. Materials

Specimens are manufactured using Hexply 8552/IM7 unidirectional prepreg material [21] for adherends and Loctite EA 9695 0.05 PSF K [25] as common high strength film adhesive for aerospace applications.

The adhesive thickness amounts to 0.2 mm for uncured conditions.

For the thermoplastic phase a poly(vinylidene fluoride) (PVDF) film material [26] of 0.125 mm thickness is chosen due to its favorable properties. Furthermore, it was shown by Hou et al. that a good bond between epoxy matrix resin of composites and PVDF is achievable in a co-curing process [27] so that good adhesion behavior could be expected. Fusion of thermoset composites by implementation of thermoplastic surface layers is also called *fusion bonding of thermoset composites* as described by Deng et al. [22]. Besides its ductile behavior (elongation at break of more than 50%), the thermoplast has a melting temperature below the adherend's curing temperature of about 167° C. The low melting temperature allows the manufacturing technique that is discussed in the previous Section.

3. Material Characterization of Adhesive Systems

3.1. Uniaxial Tensile Tests

Uniaxial tensile tests according to DIN 527 [28] are carried out to determine mechanical properties of both adhesive systems. A set of 7 specimens is manufactured for both systems to allow statistical evaluation of the characteristic values derived. An extensometer is used to obtain tensile strain and transverse contraction information. All tests are carried out displacement driven with a testing speed of 2 mm per minute. The results are summarized in Table 1. The elastic modulus as well as the Poisson's ratio are

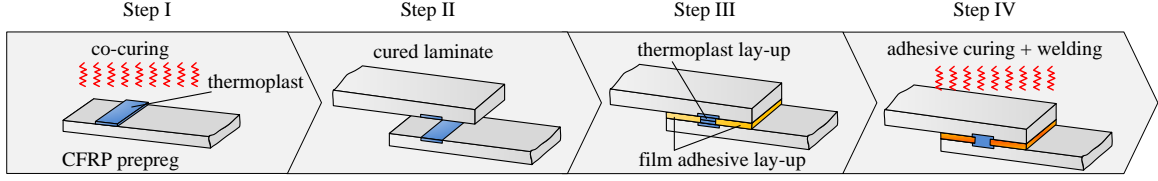


Figure 5: Manufacturing steps for hybrid (bonded & welded) joint

Table 1: Results of uni-axial material tests (averaged values)

Material property	EA9695	PVDF
Young's modulus [MPa]	2576.8	1716.1
Tensile strength [MPa]	59.2	51.5
Poisson's ratio	0.43	0.46
Global elongation at yield [%]	-	6.1
Yield strength [MPa]	-	50.7

determined between 0.05 % and 0.25 % global strain as specified by the standard.

As expected, large plastic deformations occur for the thermoplast PVDF with increasing loads. Since plasticity occurs as a local necking effect, the elongation at break can only be estimated. However, clear yielding behavior is observed in the load-displacement curves (Figure 6). By measuring the irreversible share of contraction deformation, it can be concluded that the elongation at break is greater than 50 %. The suppliers data sheet [26] states that the elongation at break amounts up to 200 %. Thus, a considerable ductile material behavior can be assumed.

The epoxy adhesive does not show plastic deformation. Material yielding by an horizontal course of the load-displacement curve does not occur.

The typical load-displacement behavior for both materials is shown by two exemplary curves in Figure 6. The comparison of the derived data shows that the thermoplast is about 33 % less stiff than the epoxy. The tensile strength is only 13 % smaller, though. Thus, the thermoplast material is capable to carry a large share of loads in case a crack grows close to the crack stopping thermoplastic zone.

3.2. Thermal Analysis

Thermogravimetric analysis (TGA) is carried out for the PVDF material to determine possible volatile

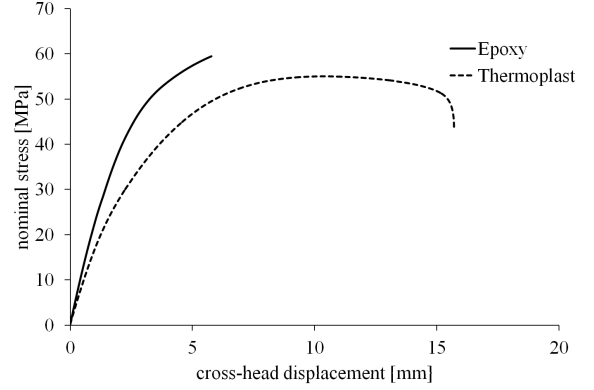


Figure 6: Load-displacement curve for both materials

components that may cause porosities during processing. The measurement is done between room temperature (20° C) and 200° C with a constant heating rate of 2 K per minute in a nitrogen atmosphere. Relative mass changes are below 0.01% over the whole temperature range. Thus, outgassing of volatile components (e.g. water) is not expected.

Differential scanning calorimetry (DSC) is carried out to determine the melting temperature of the PVDF material. The measurement is done between -80° C and 230° C with a heating rate of 10 K per minute. Melting of the material starts at 152° C and peaks at 172° C. Thus, welding of the material is feasible within the epoxy curing cycle.

3.3. Viscosity Measurements

A parallel plate viscometer is used to determine the dynamic viscosity η of both, the epoxy adhesive and the PVDF as function of temperature between room temperature (20° C) and 200° C as shown in Figure 7. The one-component epoxy reaches a minimum value of 168 Pas at approximately 110° C. At temperatures above 100° C the incorporated hardener dissolves and polymerization takes places. As the degree of cure increases, the viscosity consequently increases, too. For

temperatures above 125° C, viscosity measurements are not feasible anymore due to thermosetting.

The thermoplast in contrast does not melt below around 160° C. This correlates to the DCS results that are discussed above. The thermoplast’s minimum viscosity (120.000 Pas) is measured for the highest temperature of 200° C. At the temperature of interest (180° C) a value of 290.000 Pas is obtained.

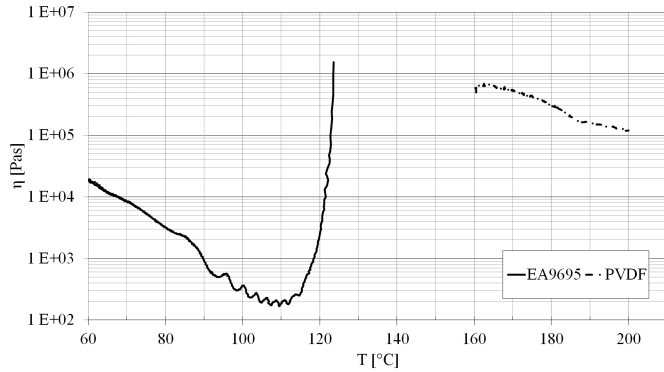


Figure 7: Dynamic viscosity of EA9695 and PVDF

It can be concluded that during the process (Section 2.2) the two systems are not simultaneously liquid. Since the PVDF’s viscosity is rather high compared to the epoxy, a substantial flow of PVDF is unlikely.

4. Manufacturing of Test Samples

4.1. Advanced Manufacturing Concept

Recent preliminary tests on the concept revealed weak adhesion in the vicinity of the thermoplastic strips [29]. An increase of porosity was observed in microsections. The fracture pattern was predominantly adhesion failure in the surrounding area of the slightly thicker thermoplast after destructive testing.

Although, the thermoplast’s influence on bonding quality is ambiguous, it is believed to be caused by an post-curing thickness mismatch. Thickness after curing amounts to merely 0.13-0.15 mm for the epoxy due to squeeze out whereas the thermoplast keeps its thickness (0.25 mm) due to its high viscosity as discussed in Section 3.3. This difference in thickness is confirmed by thickness measurements of the cured samples [29].

Porosities as another possible influence are unlikely since TGA does not reveal any volatile components

in the PVDF. Mixing of both materials is not expected as the epoxy is already cured and therefore solid before the thermoplast starts to melt.

Additional manufacturing trials by using just one PVDF film between the adherends, which equals the cured epoxy thickness, led to flow of epoxy in between the thermoplastic layers which consequently impeded proper welding.

To overcome the thickness issues, bonding is no longer done for a whole plate of 200 mm in width and cut to samples afterward. In fact, samples are cut to their width prior bonding to minimize the flow path for the rather viscous thermoplast. Preliminary trials confirm that thickness differences between the PVDF area and the conventional bonded area are considerably decreased. A visible squeeze out of PVDF material confirms material flow which reduces the PVDF’s thickness. However, a slight difference of about 0.01 mm to 0.05 mm remains. Higher pressure during bonding process may be used for larger overlap areas to constrain thickness deviations.

4.2. General Manufacturing Details

All test specimens in this study are manufactured using unidirectional prepreg material. A PTFE release film between the plates surface and the steel tooling ensures a constant overall surface finish. Curing of the prepreg system (180° C, 7 bar autoclave cycle) is done in accordance with the data sheet specifications [21].

For the preliminary tests [29], grinding was used as surface preparation of bonding surfaces. This non-uniform process also influences the adhesion and may weakens the adherend if fibers within the surface ply are damaged. Thus, in this study atmospheric pressure plasma is used as standard surface treatment to activate bonding surfaces and to ensure proper adhesion.

After cleaning with isopropanol, atmospheric pressure plasma is carried out for all test samples using a Plasmatreat plasma generator (FG5001). Optimized plasma parameters are applied that were derived in preliminary surface treatment studies. Thereby, undesired adhesion failure is avoided. For intermediate storage, activated surfaces are protected with aluminum foil. The bonding process is performed within a time frame of 24 hours after treatment to ensure

high quality bonding. As for the prepreg material, curing of the adhesive (and welding of the thermoplast) is done in an autoclave cycle (180° C, 3.5 bar) to ensure high quality bonding. Process details are shown in Figure 8 .

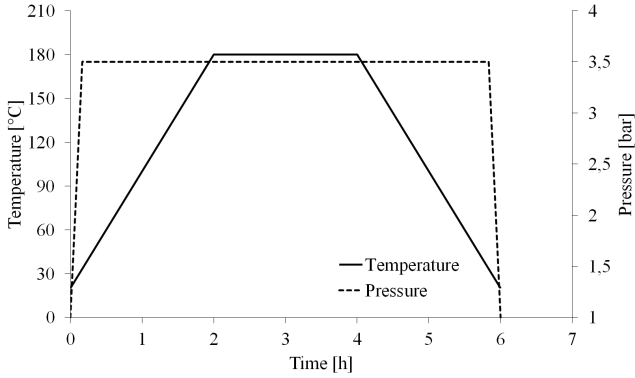


Figure 8: Autoclave bonding process

4.3. Double Cantilever Beam (DCB) Specimens

DCB specimens are manufactured and tested according to ISO 25217 test standard [30] for determination of the resistance to crack propagation under pure mode I loading conditions. Thus, those tests are suitable for a first evaluation of the disbond stopping capability. The adherends are laid in a uni-directional manner containing twelve 0°-plies orientated in longitudinal direction. With a ply thickness of 0.125 mm the overall adherend thickness amounts to 1.5 mm.

Two types of specimens are manufactured for DCB tests: 3 purely bonded samples using the epoxy film adhesive and 6 samples containing both, the PVDF strip area at a distinct position surrounded by the conventional film adhesive. The latter give an indication of the influence of the thermoplastic strip on a growing disbond. PVDF strips are inserted 65 mm from the loading point of the piano hinges (Figure 9) allowing undisturbed crack initiation and propagation in the epoxy adhesive ahead of the crack stopper and beyond.

PTFE release film of 60 mm length is inserted at one site of all DCB specimens to obtain initial delamination for fracture toughness tests as described in [30].

4.4. Single Lap Shear (SLS) Specimens

SLS tests are conducted in order to investigate the influence of the thermoplastic strips on the static

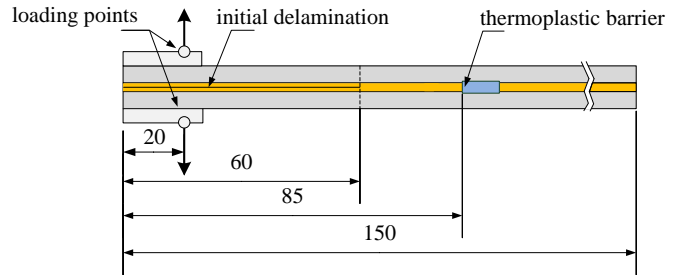


Figure 9: DCB Specimen (dimensions in mm)

strength. Similar to DCB tests, purely bonded samples, and samples containing both, a welded PVDF strip and the epoxy adhesive, are manufactured to determine their static strength. A set of five samples is manufactured for both configurations.

SLS manufacturing is done in accordance with ASTM D5868 test standard [31] with an overlap area of 25 mm by 25 mm (Figure 10). The adherend plates consist of 16 plies [0/+45/90/-45/0/+45/90/-45]_s leading to a plate thickness of 2 mm. The 0° surface plies in longitudinal direction are chosen to minimize undesired delamination failure close to the bondline while testing as described by Baker [1] and Lin et al. [32].

For samples containing PVDF, the strip is placed centrally in the overlap area. Hence, additional stress peaks are expected to be of minor impact due to low stress concentrations in the center of the overlap. In fact, experimental studies confirm that recessing of adhesive in the middle of the overlap area does hardly effect the static strength of the bond [33; 34].

Analytical stress estimations after Volkersen [35] allow to determine a reasonable maximum overlap length l^* to minimize local stress peaks within the adhesive. For an overlap length l greater than l^* , local stress concentrations at the overlap edge do not decrease anymore. The stress peak becomes independent of the overlap length. The maximum reasonable overlap length corresponds to a characteristic bonding number ρ equal to 5. This number is calculated as follows:

$$\rho = \sqrt{(1 + \Psi) \cdot \frac{G_a \cdot l^2}{E \cdot t \cdot t_a}} \quad (1)$$

The parameters needed for calculating ρ are the shear modulus of the adhesive ($G_a = 900 \text{ MPa}$), the adherend's thickness ($t = 2 \text{ mm}$) and tensile modulus ($E = 67\,419 \text{ MPa}$), the bondline thickness ($t_a = 0.15 \text{ mm}$), and the adherend's stiffness ratio Ψ . Since, both adherends are equal in thickness and stiffness, Ψ is equal to 1. The tensile modulus of the adherends is calculated by use of classical laminate plate theory.

The calculated overlap length l^* that corresponds to $\rho = 5$ equals to 17 mm. Since the welded PVDF strips have a width of 7 mm, the remaining bonded epoxy overlap length amounts to 18 mm. Thus, the hybrid bond and the reference sample should achieve comparable strength values assuming that the presence of PVDF acts similar as a reduction of load-carrying overlap.

The strength considerations above are based on the highly simplified theory of Volkersen [35]. Thereby, a lot of influencing parameters like peel stresses, non-linear adhesive behavior or shear stiffness of the adherends are neglected. However, the calculations give a reasonable estimation of the PVDF's influence on the bond strength in comparison to reference samples.

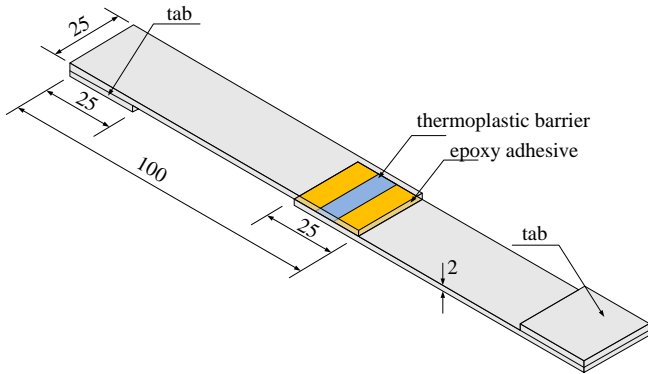


Figure 10: SLS Specimen (dimensions in mm)

5. Bondline examinations

5.1. Microsections

The advanced manufacturing process of the disbond stopping concept is examined (amongst the mechanical performance) by means of microscopic inspection. A microsection of the transition between bonded epoxy and welded thermoplast is shown in Figure 11.

The thickness of the adhesive layer only slightly increases in the vicinity of the PVDF from 0.13 mm to around 0.18 mm. Small porosities occur for some samples within the welded area. However, the number of porosities is minor. Moreover, porosities do not occur anymore within the epoxy as examined for the first trials in [29].

A resin rich area of the prepreg's epoxy matrix is formed at the edge between the thermoplastic surface ply due to slightly deflected fibers near the surface. The welded thermoplast strips do not mix with the epoxy. This was expected since rheological investigations revealed that both materials are not simultaneously liquid. As illustrated in Figure 8, heating from 120° C to the PVDF's melting temperature of around 170° C takes about 40 minutes. Hence, the epoxy adhesive is almost fully cured before the thermoplast melts.

5.2. Co-Curing Interphase

The overall performance of the hybrid bondline concept relies on the interphase between the thermoplast and the composite matrix resin. According to data sheet specifications [21], the curing cycle includes a stage of 1 hours at 110° C before the temperature is increased to 180° C. Thus, it is assumed that the CFRP matrix resin (8552) and the PVDF are also (as both adhesive systems) not simultaneously liquid since polymerization and melting temperature are reached one after another. Nevertheless, preliminary mechanical test trials revealed good adhesion between both materials. For this reason, the actual transition zone is studied in more detail.

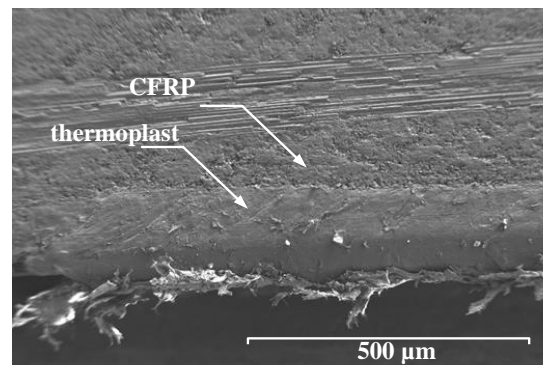


Figure 12: SEM image of transition zone

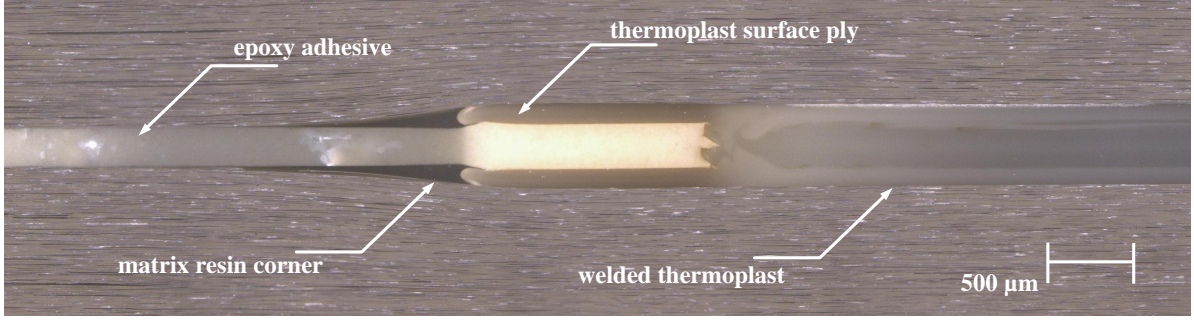


Figure 11: Microsection of hybrid bondline: transition between epoxy (bright) and thermoplastic DSF (dark)

Occurring interdiffusion of molecules (typically in a range between 10 and 1000 Å), is highly dependent on molecular weight, structure, temperature, and the thermodynamic miscibility of the polymers [22].

Scanning electron microscopy (SEM) images indicate a rather narrow transition and no distinct interdiffusion zone (Figure 12). Since PVDF is a fluorine-containing thermoplast, the fluorine content is used in energy-dispersive X-Ray analysis to study the material transition. A change of fluorine content from about 5% to about 35% is measured within 1 μm by examining the transition zone between 8552 matrix and PVDF as shown in Figure 13. Therefore, an interdiffusion of large extent can be excluded as adhesion mechanism. A semi-interpenetrating polymer network in a micrometer range is not detected.

Dohany [36] reported about the polarity of PVDF and its thermodynamic compatibility with other polymers. In fact, strong dipolar interactions are believed to make a substantial contribution to the adhesion mechanism since both, the epoxy matrix and the PVDF possess polar groups.

6. Static Test Results

6.1. DCB Results

The test setup for both static tests (DCB and SLS) is shown in Figure 14.

For DCB samples, all tests are carried out displacement driven with a testing speed of 2 mm per minute. Crack growth is recorded by use of a traveling digital microscope.

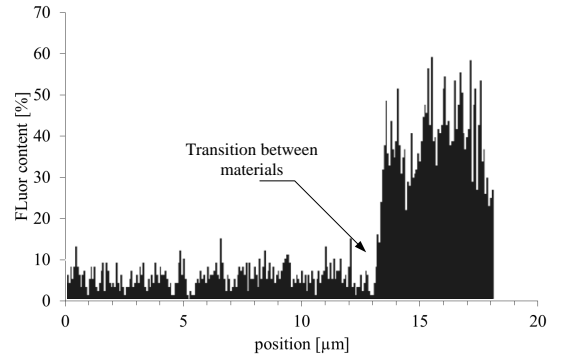


Figure 13: EDX results: Fluorine content [%] at the transition of both materials (8552 and PVDF)

The tests are carried out in two consecutive steps. In the pre-cracking stage, the specimens are loaded until a crack movement from the inserted release film is observed. This step ensures a defined crack tip within the adhesive itself. Subsequently, the specimens are re-loaded for adhesive fracture energy (critical strain energy release rate - SERR) determination as specified by the standard [30]. Since stick-slip behavior occurs for some specimens, only the simple beam theory (SBT) method is used for determination of fracture energy values. The critical energy release rate G_{IC} is calculated as follows:

$$G_{IC} = \left(\frac{3a^2}{h^3} + \frac{1}{h} \right) \cdot \frac{4P^2}{EB^2} \quad (2)$$

The parameters needed for calculating G_{IC} are specimen's width B , specimen's beam height h , load P at crack length a and tensile modulus E of the adherend.

The SERR for the reference samples is calculated to an average value of 728.5 J/m².

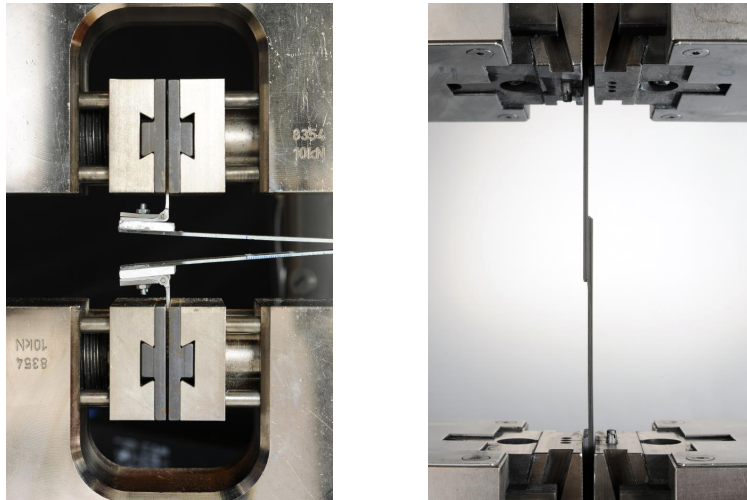


Figure 14: Mechanical test setup. left: DCB test; right: SLS test

The influence of the PVDF phase becomes visible by plotting applied load versus measured crack length (Figure 15). Up to a crack length of 45 mm, no influence becomes evident and the crack growth behavior is comparable to the reference samples. Between crack length values of 55 mm to 65 mm stick-slip behavior (unstable crack growth) occurs for all specimens containing PVDF leading to SERR of 613.3 J/m^2 which is below the reference. However, when the PVDF-barrier is reached (65 mm) very large loads are needed to force further crack growth. An average value of 124.8 N (69 % above reference) is measured before spontaneous overall unstable failure occurs. By calculating the SERR for this initiation point of further crack growth, a very large value of 2075.3 J/m^2 is obtained.

Both adhesives failed in a cohesive manner for all specimens tested (Figure 16). Although failing cohesively, the PVDF's fracture surface looks remarkable smooth and does not show clearly visible indications of plastic deformations.

6.2. SLS Results

The purely bonded reference samples show a homogeneous course of testing with minor scatter. The average ultimate load amounts to 14.62 kN with a standard deviation of 6.2%. In addition, the global failure strain level is determined to 0.46% by the use of an extensometer. The load-strain curve is linear

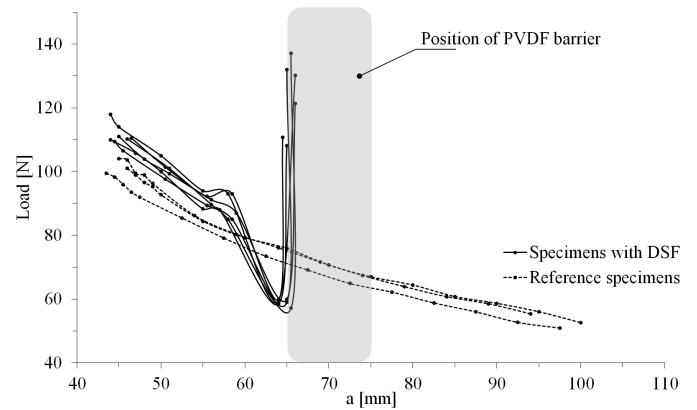


Figure 15: Load versus crack length a for specimens with and without Disbond Stopping Feature (DSF)

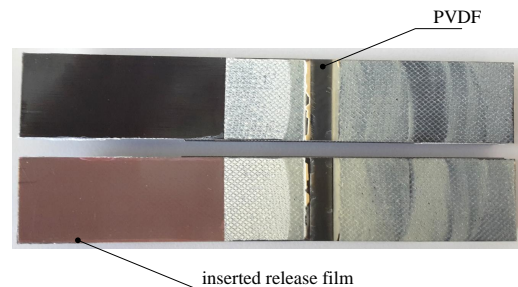


Figure 16: Fracture pattern of DCB sample

throughout the whole test for all specimens. The fracture patterns are characterized by a share of about

Table 2: Results of SLS tests

Material	Strength	Std. deviation
Reference	14.62 kN	6.2 %
DSF samples	12.14 kN	8.6 %

60-70% of cohesive failure with a simultaneous delamination of the first ply beneath the lap-bond area (first ply failure) as shown in Figure 17 (left).

PVDF containing samples on the other hand, obtain an ultimate average failure load of 12.14 kN with a standard deviation of 8.6%. As for the reference samples, all load-strain curves indicate linear behavior. The fracture pattern reveal cohesive failure for both, PVDF and the epoxy adhesive (Figure 17). The global failure strain amounts to 0.4%. A whitish coloring of the PVDF indicates plastic material deformation prior failure.

The results are summarized in Table 2.

7. Discussion

The DCB results clearly show the crack stopping capability of the concept under mode 1 loading conditions. The crack growth is significantly retarded by presence of the PVDF barrier and shifted to noticeable higher loads. However, a decrease of the resistance to crack growth is observed for about 10 mm ahead of the PVDF zone. This might be due to a slight increase of the adhesive thickness in the vicinity of the PVDF area. Additionally, stress distribution ahead of the crack tip might be disturbed due to the sharp change of materials. Thus, the material change possibly provoke an additional stress peak within the adhesive. However, this question could not be fully answered so far and is going to be investigated in more detail in subsequent studies of the actual stress distribution by the use of finite element (FE) analysis.

Since higher loads are needed before failure of the PVDF in DCB tests, a plastic deformation of the material is assumed. The deformation of the PVDF is going to be studied in subsequent studies, too. The smooth fracture surface of the PVDF though indicates a preferred and defined crack path. Thus, the weld line between the PVDF layers might be a weak link within the welded area. Using higher temperatures would lead to lower material viscosity. Thereby,

more flow of material and a better weld quality is expected.

The SLS results proof that the presence of the PVDF has only a minor influence on the overall static strength even if the epoxy overlap area a significantly reduced. Thus, the improvements in manufacturing are successful.

Fracture pattern of PVDF-containing samples suggest a higher bleed (squeeze out) of the epoxy. This is a possible reason of the measurable decreased static strength. The bleed is caused by the gap between PVDF and epoxy film. This gap is filled with the epoxy during curing process (see Figure 11). Additionally, the ratio of epoxy area to free epoxy edges decreases for the PVDF-containing samples which may also lead to an increase of bleed. Thus, negative influences of bleeding on the overall strength might decrease for larger bond areas.

Furthermore, the overall bond strength is highly dependent of the local stress peak at the overlap edge which is may influenced by bondline thickness differences. The slightly thicker bonding in the vicinity of the PVDF material may also influence the static strength of the joint. As for the DCB samples, the stress distribution within the bondline is going to be investigated in more detail in subsequent studies.

The analysis of the interphase between matrix resin and PVDF does not confirm the presence of a diffusion zone. However, the measured strength and the cohesive fracture pattern in static tests do not indicate weak adhesion. Investigation on the adhesion mechanism are going to be continued.

8. Conclusions

A novel design concept for stopping growing disbonds is introduced in this study. The suitability of a proposed combination of materials is studied in detail by means of analytical methods and static tests. By doing so, a hybrid bondline is achieved containing both, a conventional epoxy bonding area and a thermoplastic welding area. The manufacturing concept is successfully proven. The resistance to crack propagation is clearly improved as shown by mode 1 DCB tests. Thus, the concept could be promising step towards certified bonded joints of primary aircraft structures as discussed in Section 1.

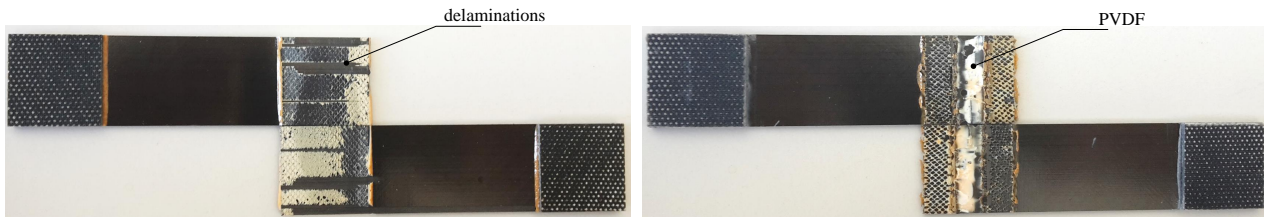


Figure 17: Fracture pattern of SLS samples: left- reference; right- sample with DSF

The adhesion mechanism between epoxy matrix and thermoplast is going to be studied in more detail in subsequent studies as well as the stress distribution of the hybrid bondline by means of FE analysis.

Furthermore, the concept is going to be validated under fatigue loading conditions in ongoing investigations which allows to study the influence of the disbond stopping feature under more realistic loading conditions.

9. Acknowledgments

The presented results are obtained within the project BOPACS of the Seventh Framework Program (FP7). The authors kindly acknowledge the European Commission for funding the research. Appreciations are extended to those who contributed to this work.

10. References

- [1] Baker AA, Dutton S, Donald K. Composite materials for aircraft structures. 2th ed. American Institute of Aeronautics and Astronautics; 2004.
- [2] Markatos DN, Tserpes KI, Rau E, Markus S, Ehrhart B, Pantelakis S. The effects of manufacturing-induced and in-service related bonding quality reduction on the mode-I fracture toughness of composite bonded joints for aeronautical use. *Composites Part B* 2013; 45: p. 556-564.
- [3] Kruse T. Bonding of CFRP Primary Aerospace Structures: Overview in the Technology Status in the Context of the Certification Boundary Conditions Addressing Needs for Development. Proceedings of the 19th International Conference on Composite Materials (ICCM/19), Montreal 2013; p. 5635-5643.
- [4] U.S. Department of Transportation - Federal Aviation Administration (FAA). Advisory Circular 20-107B Subject: Composite Aircraft Structure. FAA; 2010.
- [5] Casas-Rodriguez JP, Ashcroft IA, Silberschmidt VV. Damage in adhesively bonded CFRP joints: Sinusoidal and impact-fatigue. *Compos. Sci. Technol.* 2008; 68(13): p. 2663-2670.
- [6] Ashcroft IA, Abdel Wahab MM, Crocombe AD, Hughes DJ, Shaw SJ. The effect of environment on the fatigue of bonded composite joints. Part 1: testing and fractography. *Composites Part A* 2001; 32(1): p. 45-58.
- [7] Datla NV, Papini M, Schroeder JA, Spelt JK. Modified DCB and CLS specimens for mixed-mode fatigue testing of adhesively bonded thin sheets. *Int. J. Adhes. Adhes.* 2010; 30(6): p. 439-447.
- [8] Elder D, Qi B. High strain rate behavior of bonded composite joints. In: Camanho P, Tong L, editors. *Composite joints and connections*, Cambridge: Woodhead Publishing; 2011, p. 484-507.
- [9] Tomblin J, Strole K, Dodosh G, Ilcewitz L. Assessment of Industry Practices for Aircraft Bonded joints and Structures. FAA Report DOT/FAA/AR-05/13, Washington, 2005.
- [10] European Aviation Safety Agency (EASA). AMC 20-29 Annex II to ED Decision 2010/003/R of 19/07/2010. EASA, 2009.
- [11] Ehrhart B, Ecault R, Touchard F, Boustie M, Berthe L, Bockenheimer C et al. Development of a laser shock adhesion test for the assessment of weak adhesive bonded CFRP structures. *Int. J. Adhes. Adhes.* 2014; 52: p. 57-65.
- [12] Sachse, R, Picket, AK, Käß, M, Middendorf P. Numerical simulation of fatigue crack growth in the adhesive bondline of hybrid CFRP joints. Proceedings of the Conference on the Mechanical Response of Composites (ECCOMAS), Bristol 2015.
- [13] Löbel T, Kolesnikov B, Scheffler S, Hühne C. Enhanced tensile strength of composite joints by using staple-like pins: Working principles and experimental validation. *Compos. Struct.* 2013, 106: p. 453-460.
- [14] Kruse T, Körwien T, Heckner S, Geistbeck M. Bonding of Primary Aerospace Structures - Crackstopping in Composite Bonded Joints under Fatigue. Proceedings of the 20th International Conference on Composite Materials (ICCM/20), Copenhagen 2015.
- [15] Ranta D, Bantia AK. Toughened epoxy adhesive modified with acrylate based liquid rubber. *Polym. Int.* 2000; 49: p. 281-287.
- [16] Kinloch AJ, Mohammed RD, Taylor AC. The effect of silica nano particles and rubber particles on the toughness of multiphase thermosetting epoxy polymers. *J. Mater. Sci. Lett.* 2005.
- [17] Malkin R, Trask RS, Bond IP. Control of unstable crack propagation through bio-inspired interface modification. *Composites Part A* 2013; 46: p. 122-130.

- [18] Stapleton SE, Waas AM, Arnold SM. Functionally graded adhesives for composite joints. *Int. J. Adhes. Adhes.* 2012; 35: p. 36-49.
- [19] Da Silva LFM, Pironi A, Öchsner A. Hybrid adhesive joints. first ed. Springer, 2011.
- [20] Paton R, Hou M, Beehag A, Falzon P. A Breakthrough in the Assembly of Aircraft Composite Structures. Proceedings of the 25th International Congress of the Aeronautical Science (ICAS 25), Hamburg 2006.
- [21] Hexcel. HexPly 8552 epoxy matrix product data. Hexcel Composites Publication; 2012.
- [22] Deng S, Djukic L, Paton R, Ye L. Thermoplastic-epoxy interactions and their potential applications in joining composite structures - A review. *Composites Part A* 2015; 68: p. 121-132.
- [23] Hou M. Fusion Bonding of Carbon Fiber Reinforced Epoxy Laminates. *Adv. Mater. Res.* 2013; 626: p.250-254.
- [24] Yang F, Pitchumani R. Interlaminar contact development during thermoplastic fusion bonding. *Polym. Eng. Sci.* 2002; 42: p. 424-438.
- [25] Henkel. Loctite EA9695 Aero Epoxy Film Adhesive - Technical Process Bulletin. Henkel Corporation. 2013.
- [26] Arkema. Kynar & Kynar Flex PVDF - Performance Characteristics & Data. Arkema Inc. 2007.
- [27] Hou M, Tang XG, Zou J, Truss R. Increase the Mechanical Performance of Polyvinylidene Fluoride (PVDF). *Adv. Mater. Res.* 2011; 393-395: p 144-148.
- [28] DIN Standard. EN ISO 527-2 Plastics- Determination of tensile properties. DIN 1996.
- [29] Löbel T, Kühn M, Holzhüter D, Hühne C. Experimental Investigations of the disbond stopping capability of a novel epoxy-thermoplastic bondline architecture for composite joints. Proceedings of the 16th European Conference on Composite Materials (ECCM 16); Seville 2014.
- [30] International Standard, ISO 25217. Adhesives - Determination of the mode I adhesive fracture energy of structural adhesive joints using double cantilever beam and tapered double cantilever beam specimens. ISO 2009.
- [31] ASTM International, ASTM D5868-01. Lap Shear Adhesion for Fiber Reinforced Plastic (FRP) Bonding. ASTM 2014.
- [32] Lin KY, Liu W. Delamination Arrest of Fasteners in Aircraft Composite Structures. Proceeding of the 19th International Conference on Composite Materials (ICCM/19); Montreal 2013; p. 1577-1580.
- [33] Lang TP, Mallick PK. The effect of recessing on the stresses in adhesively bonded single-lap joints. *Int. J. Adhes. Adhes.* 1999; 19: p. 257-271.
- [34] Hart-Smith LJ. An engineer's viewpoint on design and analysis of aircraft structural joints. Proceedings of the Institution of Mechanical Engineers, Part G: J. Aeronaut. Eng. 1995; 27: p. 105-129.
- [35] Volkersen O. Die Nietkraftverteilung in zugbeanspruchten Nietverbindungen mit konstanten Laschenquerschnitten. *Luftfahrtforschung* 1938. 15: p. 4-47.
- [36] Dohany JE, Fluor containing polymers, Poly(Venylidene Fluoride). 19th Encyclopedia of Chemical Technology. Kirk-Othmer; 2000.